Earthquake-induced Deformation Analysis of a TSF Undergoing Tailings Reprocessing

Paola Torres, Georgia Institute of Technology, USA
Jorge Macedo, Georgia Institute of Technology, USA
Solange Paihua, Knight Piésold Consultores, Peru

Abstract

This study discusses advanced, effective stress analyses conducted to assess the seismic performance of a tailings storage facility (TSF) undergoing re-handling and reprocessing of tailings. The deposited tailings are expected to contain high residual mineral values, which has prompted the reprocessing operation. In this context, the seismic stability of the TSF is of interest as it is situated in a high seismicity area in the South American Andes, where subduction earthquakes are known to occur. The TSF is a legacy mining facility developed with the upstream construction method, and it has not been in operation for many years. Nevertheless, the high degree of saturation level of the deposited tailings makes it susceptible to liquefaction. Moreover, since the reprocessing operation involves excavation, dragging, and re-handling of tailings, the effects of earthquake-induced deformations must be considered for the operation planning.

The material strength and dynamic properties required to conduct effective stress seismic analyses have been estimated based on geotechnical site investigations and laboratory testing programs. The characterization of the deposited tailings under considerable layering effects and spatial variability is of particular interest. The field and laboratory results are used to characterize an advanced stress ratio-based model developed within the framework of bounding surface plasticity and consistent with the critical state framework. The assessment has been developed to estimate the TSF performance in terms of deformations under design ground motions representative of the seismicity in the South American Andes. Results from the analyses and how they inform the overall TSF planning are shared.

Introduction

This paper presents dynamic effective stress analyses of an inactive tailings storage facility (TSF) in the South American Andes. The TSF is a legacy mining facility developed with the upstream construction method. The deposited tailings contain high residual mineral values, which motivated the reprocessing operation. Since the reprocessing activities involve the excavation of tailings with a high degree of

saturation, geotechnical assessments are needed to ensure the operation is feasible and can be safely executed. This paper is limited to earthquake-induced deformation analyses of the TSF. At the time the analyses were performed, the TSF had a downstream slope of 7H:1V, a shoulder length of 250 m, and a height of 22 m.

The geotechnical site investigations included boreholes, RSCPTu, and a geophysical survey campaign. It provided information regarding the TSF saturation condition and the in-situ state and strength of the tailings. It was found that the water level estimated with piezometers did not necessarily agree with a low saturation level. This disagreement was caused by the retention of water in fine-grained tailings. A thorough laboratory testing program was executed to characterize the tailings and serve as inputs for the constitutive models used in the analyses.

Finally, we performed fully coupled stress-flow dynamic analyses using design ground motions provided by a probabilistic seismic hazard study (PSHA). The UHS for 100 and 475 years of return periods were considered in the design criteria for TSF reprocessing. The cyclic shear-strain behaviour of the tailings was captured by the constitutive model PM4Silt (Boulanger and Ziotopoulou, 2018). For the nonlinear behaviour of the non-liquefiable material in the foundation, UBCHYST (Naesgaard, 2011) was employed. Both models are user-defined constitutive models available in FLAC 8.1 (Itasca, 2016).

Description of the tailings and foundation materials

The TSF is mostly comprised of tailings deposited over a foundation composed of lacustrine clays, moraine, residual soil, and bedrock. Figure 1 shows the plan view of the TSF, along with the cross-section used in the analyses. Figure 2 shows the distribution of tailings and foundation materials, as well as the nomenclature used to describe the TSF zones in this paper.

Foundation

Lacustrine clays are composed of gravelly fat clays (CH) and gravelly lean clays (CL). Their consistency varies from firm to very stiff; however, a soft layer was identified below the south slope toe. CPTu and vane shear tests were used to estimate peak and residual undrained shear strengths. Moraine predominantly comprises clayey gravels (GC) and silty and clayey sands with gravels (SC/SM). Their compactness varies from medium to very dense. Below the clays and moraine layers, a layer of residual soil consisting of extremely weathered slate rock can be found. Finally, the bedrock is composed of slate rock, which ranges from moderately to slightly weathered with depth.

Tailings

The particle size distribution of tailings varies across the deposit extent, showing spatial variability and

layering. This study grouped tailings into three types: silty sands, sandy silts, and fines. Standard laboratory testing to characterize tailings was performed, particularly to determine the water content (ω%) in all samples recovered every 1 m from drill boreholes. We estimated the unit weight with CPT correlations, and then, by using the water content and specific gravity (Gs), the degree of saturation (Sr%) was obtained. Similarly, the in-situ void ratio was estimated based on Gs, unit weight, and water content. Table 1 presents the main characteristics of tailings.

Moreover, a complete set of advanced laboratory tests was conducted. This program included undrained and drained triaxial shear tests (CUTX and CDTX), cyclic simple shear tests (CSS), bender element tests, monotonic simple shear tests (DSS), constant rate strain consolidation tests, and soil-water characteristic curve (SWCC) tests. Triaxial shear tests were employed to determine the critical state line (CSL) of the tailings at different degrees of saturation. Based on the estimated void ratio, the in-situ mean effective stress (p'), and the CSLs, the state parameter (ψ) was estimated for different Sr%. This information was later used to estimate the Sr% by which the tailings could still be susceptible to liquefaction.

Silty sands

This type of tailing is composed of sand and has an average fines content (FC%) (i.e., particles below mesh #200) of 30%. It is classified as silty sand (SM) with non-plastic fines. According to the NSPT blow count, its compactness varies from loose to medium dense (Terzagui and Peck, 1948). The Sr% is lower than 45% in samples above the water table. For deeper depths, the Sr% varies between 50% and 85%. Based on the SBT chart from Robertson (2016), most silty sands are in the sand-like zone, in the contractive (SC) and dilative (SC) areas. Figure 3 shows soil behaviour type (SBT) charts for tailings.

Sandy silts

This type of tailing is composed of sandy silts and silts with sands (ML). The average FC% is 60%. Plasticity is low, with a plasticity index (IP) lower than 4. The tailings compacity varies from soft to stiff. The Sr% is lower than 45% in samples above the water table. However, in most samples, the Sr% varies between 65% and 90%, even above the water table in the center zone of the deposit. Based on the SBT chart, this type of tailings can behave sand-like or clay-like, depending on the sand content of the material.

Fines

This type of tailing is composed of silts (ML), silty clays (CL-ML), and lean clays (CL). The average FC% of the silts and silty clays is 90%, and the IP is lower than 7 and can be found in the south of the deposit, while clays have an average fine content of 99 % and an IP between 10 and 17 and can be found in the north. The compacity is very soft. The Sr% is higher than 90% in samples from the north zone. The Sr%

varies between 70% and 90% in the central zone. Based on the SBT chart, most fine tailings are in the clay-like zone, in the contractive (CC) and contractive-sensitive (CCS) areas.

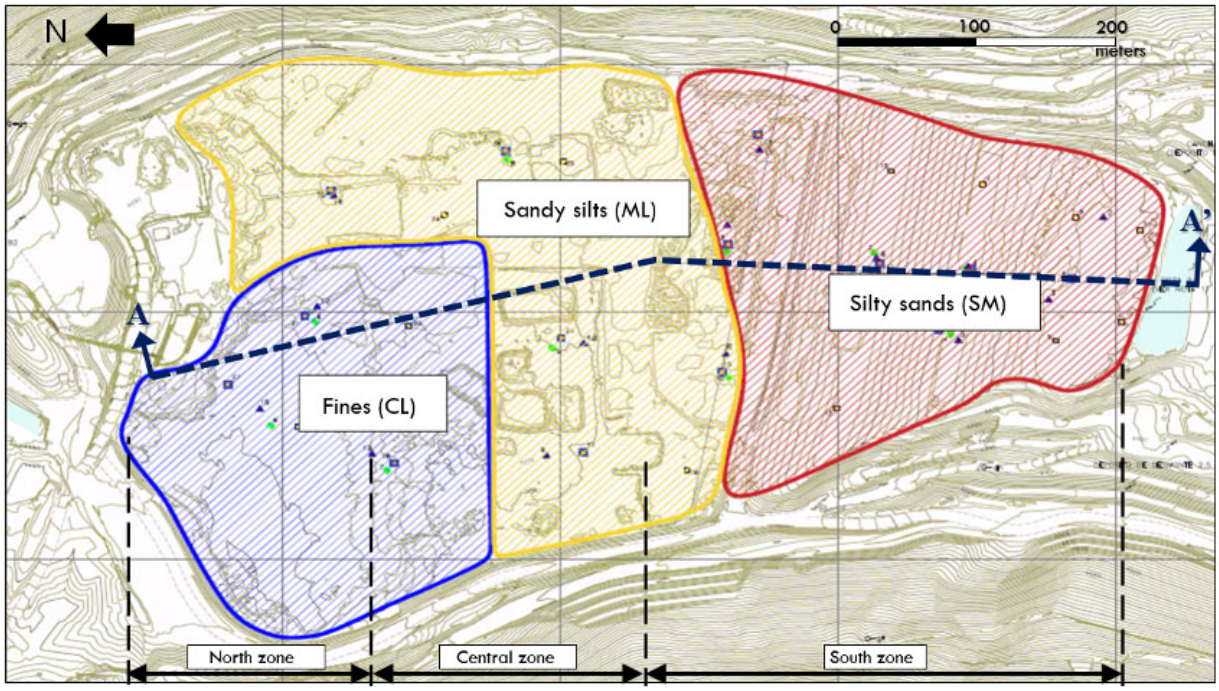

Figure 1: Plan view of the TSF

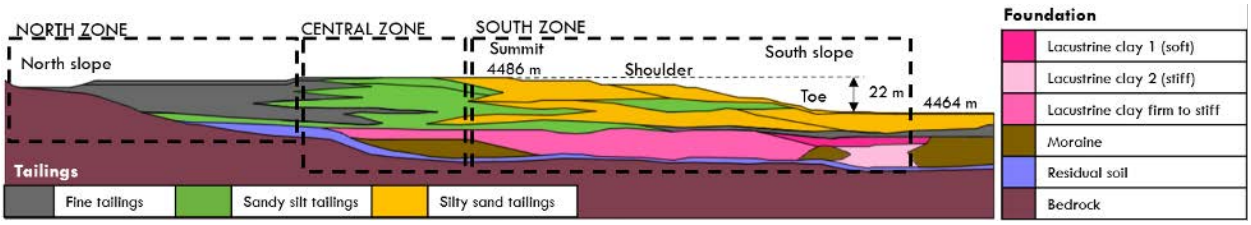

Figure 2: Cross-section A-A'

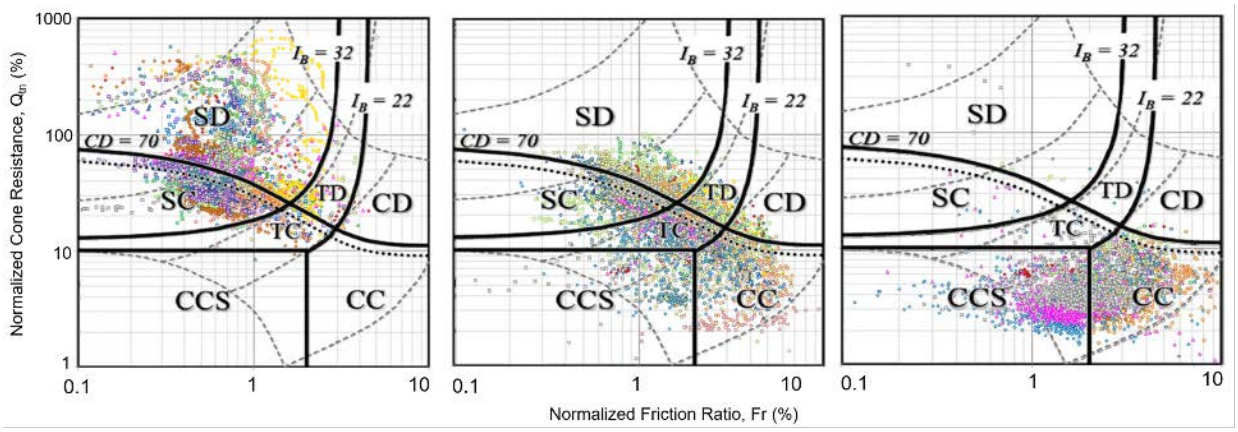

Figure 3: SBT chart for the silty sands, sandy silts, and fine tailings (from left to right)

Table 1: Tailings characterization

	Silty sands tailings	Sandy silts tailings	Fine tailings
Specific gravity, Gs	2.80	2.83	2.90
N_{SPT} blow count	5 – 18	2 – 10	0 – 2
Cone resistance tip, q_t (MPa)	2 – 15	1 – 10	0.1 – 2
Shear wave velocity, Vs (m/s)	120 – 250	120 – 140	70 – 180 (depth <18 m) 180 – 250
In-situ void ratio, e	0.50 – 0.80	0.65 – 1.10	0.9 – 1.20

Numerical model and initial stresses before seismic loading

The software used for the numerical analyses was FLAC 8.1, which solves stress-strain problems with a fully explicit time-marching numerical formulation in 2D dimensions. For this study, we employed a variable height for the finite difference elements, ranging from 1 to 3 m for softer to stiffer materials. We also used a uniform width of 1 m for all elements. The FLAC model dimensions are shown in Figure 4.

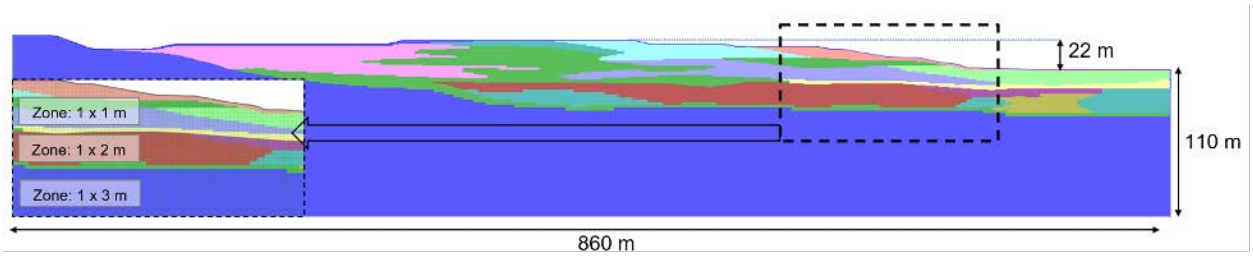

Figure 4: FLAC numerical model of the TSF

Later, the model was analyzed under gravity loads with drained conditions to establish the pre-earthquake stress state. Mechanical analyses are run until equilibrium is reached in each modelling stage. The Mohr-Coulomb model was assigned to the tailings and foundation materials, while the elastic model was assigned to the bedrock. We estimated the shear modulus of the materials based on the Vs obtained by geophysical methods in the field. In total, 15 materials were employed in the numerical model. The three main groups of tailings were subdivided because of spatial variability and their dilatory or contractive behaviour. Table 2 summarizes the material properties used in the numerical model.

Along with the static analyses, flow analyses were performed to obtain the steady-state flow condition and initiate the pore water pressures of the model. Groundwater boundary conditions were applied to the model to obtain a water table that simulated the desired fully saturated zones. The full saturation scenario was defined not only according to water level but more importantly, according to the degree of saturation threshold estimated for contractive behaviour in tailings. This scenario is shown in Figure 5.

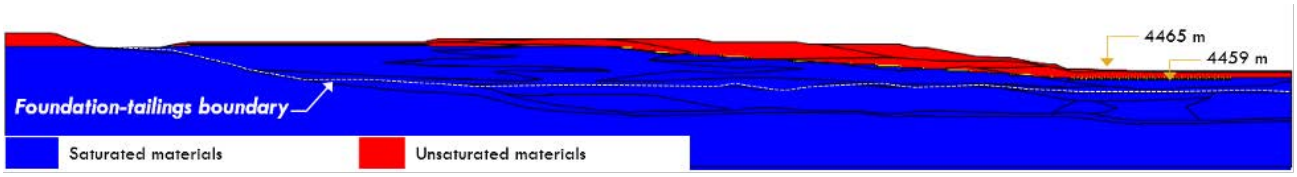

Figure 5: Saturation scenario for the numerical model

Table 2: Material properties for static and flow analysis

Material	Dry unit weight γ_{dry} (kN/m³)	Friction angle ϕ' (°)	Cohesion c (kPa)	Poisson ratio ν	Shear stiffness G* (MPa)	Bulk Modulus K** (MPa)	Porosity n	Hydraulic conductivity k (m/s)
Silty sands tailings	15.4–16.5	28–30	0	0.30	48–89	105–192	0.40–0.44	6E-6–7E-7
Sandy silts tailings	15.4	28	0	0.33	44–79	108–205	0.44	2.5E-7
Fine tailings	13.3–14.9	26–30	0	0.40	15–85	69–397	0.48–0.53	2E-9
Lacustrine clay (firm to stiff)	14.9	0	85	0.40	143	666	0.46	1E-8
Lacustrine clay 1	12.5	0	35	0.40	39	182	0.54	1E-8
Lacustrine clay 2	14.9	0	75	0.40	251	1,170	0.46	1E-8
Moraine	19.5	34	5	0.35	510	1,530	0.30	1E-8

*Static shear stiffness (G) was taken as $0.1G_{max}$. G_{max} is the small strain shear modulus estimated as $G_{max}= \rho V_s^2$, where ρ is the total density of the material.

**Bulk modulus (K) is calculated as K=G*2*(1+ ν)/(3*(1-2 ν)).

Constitutive models

Non-liquefiable materials

The UBCHYST constitutive model was selected for foundation materials, dilative and non-saturated tailings. These materials are considered non-liquefiable due to their particle size, compaction degree, or unsaturated condition. The non-linear hysteretic UBCHYST is a robust, relatively simple, total stress model. It uses the Mohr–Coulomb failure criterion, extended with a formulation for reducing the shear secant modulus with strain and the emulation of marching or ratcheting occurring when there is a static shear bias (Naesgaard, 2011). Typically, the model is used for fine-grained soils (silts and clays) with undrained strength parameters, free-draining granular soils with drained strength parameters, or unsaturated granular soils.

One of the input parameters for the dynamic analysis is the small strain (dynamic) shear modulus, G_{max}, which was estimated from the materials density and Vs. Variable values of G_{max} were applied according to the effective confinement stress of the materials following Equation 1 for coarse-grained materials, which was proposed by Seed et al. (1986), and Equation 2 for clays, proposed by Hardin (1978),

$$G_{max} = 21.7\, k_{2,max}\, (\sigma'_m Pa)^{0.5} \quad \text{(Eq. 1)}$$

where G_{max}, $k_{2,max}$, P_a and σ'_m are the small strain shear modulus, modulus coefficient, atmospheric pressure, and the mean confining pressure, respectively.

$$G_{max} = \frac{625}{0.3+0.7e^2}\ (\sigma'_m Pa)^{0.5}\, OCR^k \quad \text{(Eq. 2)}$$

where e, OCR, and k is the void ratio, over-consolidation ratio and a parameter that depends on the index plasticity (IP), respectively.

The UBSHYST model was calibrated for each material to simulate the normalized shear modulus degradation curve and the damping ratio curve. These curves were selected according to soil characteristics. The curves used in this study were based on Rollins et al. (1998) and Darendeli (2001). Table 3 presents the summary table of material properties for non-liquefiable materials.

Table 3: Input parameters for non-liquefiable materials

Material	Dry unit weight γ_{dry} (kN/m3)	Modulus coefficient $k_{2,max}$	OCR	Void ratio e	Small strain shear modulus G_{max} @1 atm (MPa)	Bulk modulus K_{max} @1 atm (MPa)	UBCHYST* Input parameters H_n	H_{rf}	H_{rm}	H_{dfac}
Silty sands tailings	16.5	**30**	–	–	**66**	**143**	**2.7**	**0.98**	**1.0**	**0.8**
Sandy silts tailings	15.4	**25**	–	–	**55**	**143**	**3.3**	**0.98**	**1.0**	**0.8**
Fine tailings	13.2	–	**1**	**1.30**	**43**	**199**	**3.7**	**0.90**	**1.0**	**0.8**
Lacustrine clay (firm to stiff)	14.9	–	**1**	**0.85**	**79**	**367**	**1.0**	**0.70**	**2.5**	**0.8**
Lacustrine clay 1	12.5	–	**1**	**1.00**	**63**	**295**	**1.0**	**0.70**	**1.0**	**0.4**
Lacustrine clay 2	14.9	–	**5**	**0.50**	**184**	**856**	**1.0**	**0.70**	**3.0**	**0.0**
Moraine	19.5	**150**	–	–	**330**	**989**	**1.1**	**0.70**	**3.0**	**0.8**

*The calibration parameter H_{modf1} is 1 for all materials.

Liquefiable materials

On the other hand, the PM4Silt constitutive model was selected for tailing materials expected to be susceptible to liquefaction due to their loose state or saturation degree. PM4Silt is a stress-ratio-based, critical-state-consistent model formulated under the framework of bounding surface plasticity. PM4Silt was developed by Boulanger and Ziotopoulou (2018) to represent the cyclic behaviour of low-plasticity silts and clays. The input parameters of the constitutive model can be adjusted accordingly to obtain a better match with the laboratory-based liquefaction resistance curves and the shear-strain response observed in the CSS tests. The results of laboratory experiments were used to calibrate the PM4Silt constitutive model.

The liquefaction resistance curve (i.e., cyclic stress ratio [CSR] versus the number of cycles for liquefaction) was defined by multiple CSS tests executed for the three types of tailings (Figure 6). As observed in the literature for tailings with similar characteristics (Macedo et al., 2022), the slope of the liquefaction resistance curves (LRCs) is quite flat, showing fitted power exponent values lower than 0.2. It was also found that the increment in the consolidation stress slightly raises the resistance of the fine tailings. In contrast, the liquefaction curve remained insensitive for the silty sands and sandy silts. This behaviour has been observed in previous publications like Wijewickreme et al. (2005), Riemer et al. (2017), and Macedo et al. (2022). This effect may be related to the compressible nature of the fine tailings, as there is a general trend for densities to be higher as confinement stresses increase.

The undrained shear strength ratio at critical state ($S_{u,cs/\sigma' vc}$) values were estimated from DSS tests or the CPTu soundings, but it was modified later to obtain a better fit with the laboratory-based LCRs. The bounding surface parameter ($n_{b,wet}$) was set to 1.0 because this limits the peak shear resistance to $S_{u,cs,eq}$ in the simulation, which matches the strain-hardening response observed in the DSS test. Moreover, the shear modulus coefficient (G_o) and shear modulus exponent (n_G) values were obtained from the bender element test results. Finally, the critical friction angle (φ_{cv}) and the compressibility in e-ln(p') space (λ) were obtained from the critical state line (CLS) generated from the triaxial shear test with 100% saturation condition.

Based on previously defined parameters, undrained cyclic loading was simulated on FLAC to find the contraction rate parameter (h_{po}) value that would best adjust the fit to the LCRs. We also compared the stress-strain and stress-path responses in the CSS test and numerical simulations. As a result, the secondary parameters were modified to flatten the liquefaction resistance curve. They were also modified to generate stress-strain and excess pore-pressure responses like those experimentally observed. Table 4 summarizes the input parameters for the PM4Silt model. Figure 6 shows CSS test results and simulated LRCs.

Table 4: Input parameters for PM4Silt calibrations for tailings

Input parameters		Default value	Calibration parameters		
			Silty sands tailings	Sandy silts tailings	Fine tailings
Primary parameters					
Undrained shear strength ratio at critical state	$S_{u,cs}/\sigma'_{vc}$	–	0.18	0.18	0.18
Shear modulus coefficient	G_o	–	790	568	411
Contraction rate parameter	h_{po}	–	3.7	2.0	3.0
Secondary parameters*					
Initial void ratio	e_o	0.9	0.7	0.8	1.0
Shear modulus exponent	n_G	0.75	0.722	0.721	0.765
Critical state friction angle	ϕ_{cv}	32	35	34.8	34.6
Compressibility in e-ln(p') space	λ	0.06	0.035	0.039	0.059
Sets bounding p_{min}	$r_{u,max}$	$p_{min}=p_{cs}/8$	Default	0.99	0.99
Bounding surface parameter	$n^{b,wet}$	0.8	1	1	1
Dilatancy parameter	A_{do}	0.8	Default	Default	0.4
Fabric growth parameter	c_z	100	75	175	75
Strain accumulation rate factor	$c\xi$	$0.5\leq(1.2Su/\sigma'_{vc}+0.2)\leq1.3$	1.0	Default	0.9

* The secondary parameters not included in the table were kept with the default value.

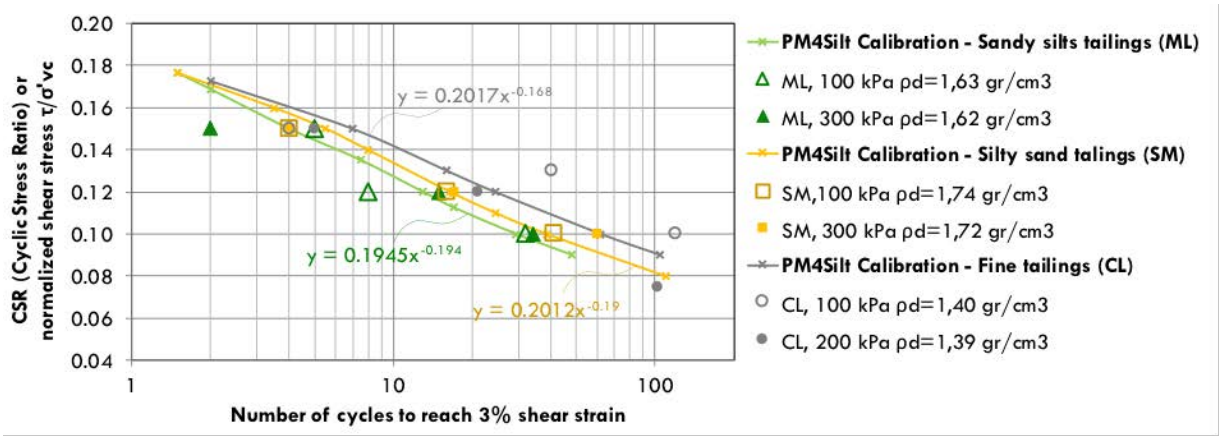

Figure 6: CSR versus number of uniform loading cycles to cause 3% shear strain in undrained cyclic simple shear tests and the PM4Silt simulations for the LCRs

Time histories – examples

According to the site seismic disaggregation analysis, earthquakes of moderate magnitude corresponding to the intra-slab subduction mechanism are the largest contributors to the seismic hazard. However, high-

magnitude earthquakes corresponding to the interface subduction mechanism also contribute. Figure 7 shows two representative seismic records of the two types of subduction settings used in the analyses: Arica (2005) and Lima (1974). We selected the spectrally matched earthquakes for a return period of 100 (PGA = 0.12g) and 475 years (PGA = 0.22g), which we considered appropriate for the period of the tailings reprocessing, approximately eight years.

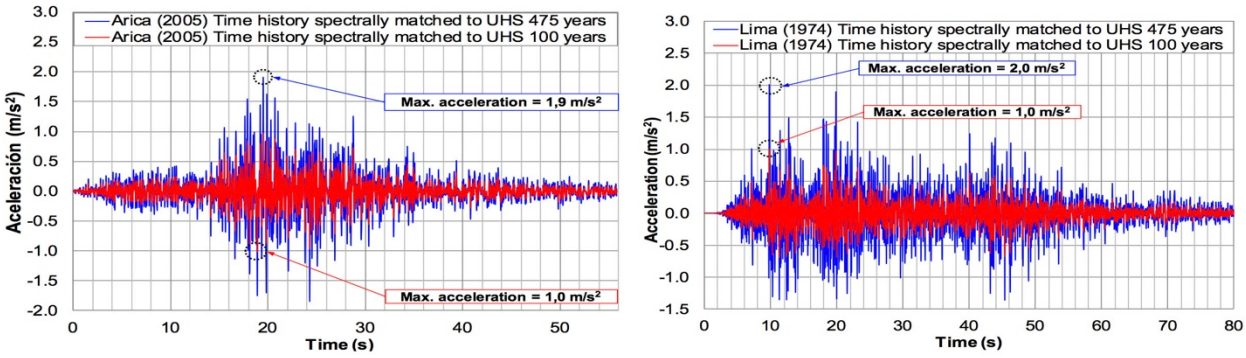

Figure 7: Acceleration time-histories adjusted to the design MCE acceleration spectrum

Results and discussion

Dynamic effective stress analysis: end-of-shaking and post-seismic phase

This section presents the results for one of the case scenarios analyzed. The results at the end-of-shaking and post-seismic phase are shown in Figures 8 to 9. At the end-of-shaking, we obtained displacements of 1.5 m on the south slope toe and 30 cm in the central zone. Then, following a criterion defined on excess pore pressure (Ru>0.7) or the shear strain deformation level experienced by these materials, residual undrained shear strength was assigned to tailings and lacustrine clays after the seismic event. In the post-seismic phase, displacements around 6 m at the toe and 1 m on the shoulder of the south slope were obtained in the horizontal direction. Further, the shear strains increased considerably in the post-seismic phase, indicating a rotational failure of the south and north slopes. The equilibrium could not be reached in FLAC because of mesh limitations to reach large deformations, but these results indicate an ongoing landslide.

In this study, two return periods were considered. The analyses corresponding to a 475-year return period show ongoing failure of the north and south slopes, and the model did not stabilize in FLAC. Moreover, it can be observed that the summit is affected by the ongoing south slope deformations. On the other hand, for a 100-year return period, results show a local movement of the south slope, and displacements and deformations stabilize in the post-seismic phase. However, there is still an ongoing landslide on the north slope (~5 m height). The summit and central zones of the TSF are not affected by the south slope displacements and deformations (<10 cm). Figure 9 shows a comparison of these results.

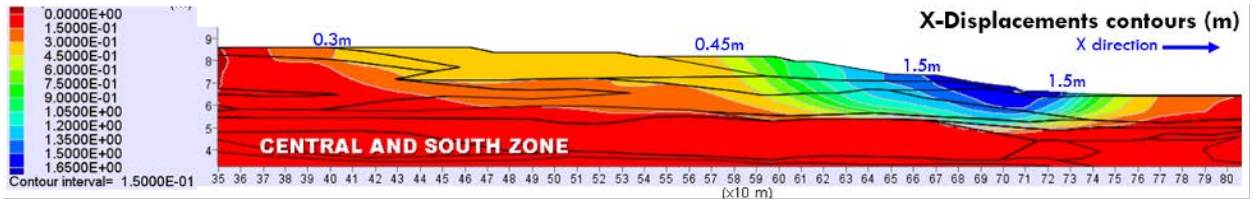

Figure 8: Horizontal displacements at the end-of-shaking.
Case scenario: Ground motion Lima (1974) – 475 year return period

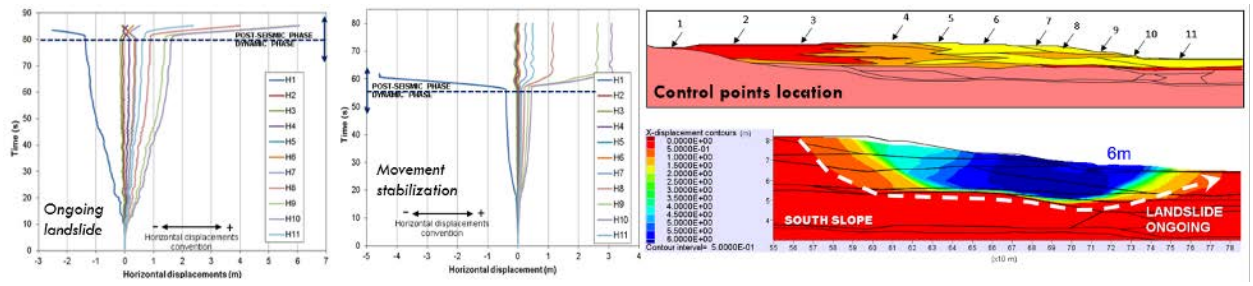

Figure 9: Horizontal displacements comparison: ongoing landslides for a 475-year return period and movement stabilization for a 100-year return period

Summary and conclusions

The results of this study indicate that earthquake-induced deformations are limited in the case of a 100-year return period ground motion. However, in the case of a 475-year return period, inadequate performance of the north and south slopes is expected. These results were inputs for the risk assessments performed for the reprocessing planning operation. These analyses allowed us to identify mobilized zones during and after an earthquake, which helped to optimize the earthquake evacuation plans for mining operators.

It is important to acknowledge that the analyses conducted were limited to small to moderate deformations (less than 10 m); numerical large deformation schemes would be required to deal with large deformations. Further, the saturation assessments helped to define the saturation scenario used in the earthquake-induced deformation analyses. While the water table did not precisely align with the potential areas of the tailings exhibiting contractive behaviour under shearing, implying liquefaction susceptibility, it became apparent that a more comprehensive understanding of the tailings' saturation conditions was necessary. Nevertheless, a constraint exists concerning the constitutive models employed for partially saturated conditions in dynamic numerical simulations. Therefore, a fully saturated scenario was used.

Acknowledgement

We thank Mr. Ruben Vargas from Knight Piésold Consultores for providing valuable comments for this study.

References

Boulanger, R.W. and Ziotopoulou, K. 2018. PM4Silt (Version 1): A silt plasticity model for earthquake engineering applications. Report No. UCD/CGM-18/01, Center for Geotechnical Modeling, Department of Civil and Environmental Engineering, University of California, Davis, CA, 108 pp.

Darendeli, M.B. 2001. Development of a new family of normalized modulus reduction and material damping curves. Doctoral thesis, University of Texas.

Hardin, B.O. 1978. The nature of stress-strain behaviour for soils. In Volume I of *Earthquake Engineering and Soil Dynamics – Proceedings of the ASCE Geotechnical Engineering Division Specialty Conference*. Pasadena, California.

Itasca. 2016. FLAC 8.0 (Fast Lagrangian Analysis of Continua) User Manual. Itasca Consulting Group, Inc., Minneapolis.

Jefferies, M. and Been, K. 2015. *Soil Liquefaction: A Critical State Approach*. CRC press.

Macedo, J., Torres, P., Vergaray, L., Paihua, S. and Arnold, C. 2022. Dynamic effective stress analysis of a centreline tailings dam under subduction earthquakes. In *Proceedings of the Institution of Civil Engineers-Geotechnical Engineering* 175(2): 224–246.

Naesgaard, E. 2011. A hybrid effective stress-total stress procedure for analyzing embankments subjected to potential liquefaction and flow. PhD thesis, Civil Engineering Department, The University of British Columbia, Vancouver, BC, Canada.

Riemer, M., Macedo, J., Roman, O. and Paihua, S. 2017. Effects of stress state on the cyclic response of mine tailings and its impact on expanding a tailings impoundment. In *The 3rd International Conference on Performance-based Design in Earthquake Geotechnical Engineering*. Vancouver.

Robertson, P.K. 2016. Cone penetration test (CPT)-based soil behaviour type (SBT) classification system – an update. *Canadian Geotechnical Journal* 53(12): 1910–1927.

Rollins, K.M., Evans, M.D., Diehl, N.B. and Daily III, W.D. 1998. Shear modulus and damping relationships for gravels. *Journal of Geotechnical and Geoenvironmental Engineering* 124(5): 396–405.

Seed, H.B., Wong, R.T., Idriss, I.M. and Tokimatsu, K. 1986. Moduli and damping factors for dynamic analyses of cohesionless soils. *Journal of Geotechnical Engineering* 112(11): 1016–1032.

Terzaghi, K. and Peck, R.B. 1948. *Soil mechanics. Engineering Practice*. John Wiley & Sons, Inc., New York.

Wijewickreme, D., Sanin, M.V. and Greenaway, G.R. 2005. Cyclic shear response of fine-grained mine tailings. *Canadian Geotechnical Journal* 42(5): 1408–1421.